

Annealing temperature effects on superduplex stainless steel UNS S32750 welded joints. II: pitting corrosion resistance evaluation

R. Cervo · P. Ferro · A. Tiziani · F. Zucchi

Received: 12 October 2009 / Accepted: 8 February 2010 / Published online: 20 February 2010
© Springer Science+Business Media, LLC 2010

Abstract This study deals with the effect of the annealing temperature on the pitting corrosion resistance of UNS S32750 submerged-arc welded joints. In a companion article (Part I), the influence of post-weld annealing temperature on microstructure evolution and chemical composition of austenite and ferrite was analyzed; this study can thus be considered directly connected with the previous one. The pitting corrosion resistance of the heat-treated welded joints was evaluated by using both electrochemical measurements and ASTM G48 standard gravimetric tests; examinations of initiation sites of pitting attack were carried out in order to correlate the experimental data obtained in this study with the predicted pitting corrosion behavior obtained by using the results described in Part I. Generally, the post-weld annealing treatment enhances the pitting corrosion resistance of UNS S32750 welded joints. By using PREN analysis of single phases, a correlation between the chemical composition evolution of ferrite and austenite and the experimental pitting behavior of the welded joints was found, in relation to welding and post-welding heat treatment temperature. In particular, an exponential relationship between PREN of weaker phase and pitting potential in 3.5% NaCl solution at 80 °C for the weld metal was obtained. The most favorable annealing temperature for the analyzed welded joints was found to be 1100 °C.

Introduction

It is well known that ferrite/austenite balance and phases' chemical composition of superduplex stainless steels (SDSS) is generally altered by welding operations [1–7], and the precipitation of detrimental phases in the reheated weld beads and heat-affected zone (HAZ) could take place [8–11]. Consequently, the excellent corrosion properties of such alloys, especially in terms of pitting corrosion resistance, could be compromised [12–15]. The diagram of Fig. 1 shows the effect of ferrite content on pitting rate, indicating the importance of phases balance control in order to obtain suitable corrosion properties [16].

In order to assure a more balanced microstructure, appropriate filler metals enriched in austenite-stabilizer elements are used during welding of DSS and SDSS [17]. However, a post-weld solution heat treatment could be required in order to restore the optimal pitting corrosion resistance of such joints [18].

The pitting corrosion of stainless steels is generally associated to a local breakdown of the protective passive layer and their susceptibility to such damage can be evaluated by using different methods: critical pitting temperature measurements, gravimetric tests after immersion in high-aggressive solutions, and electrochemical measurements. It is generally accepted that pitting initiates when the pitting potential reaches a critical value (E_p), which depends on the chemical composition of the alloy and on the environment (temperature and chloride concentration). E_p is often measured by potentiodynamic anodic polarization tests. In these measurements the onset of pitting corrosion is observed as an irreversible increase in current density (Fig. 2). The higher the E_p value, the more resistant is the alloy to pitting corrosion in the environment considered [19].

R. Cervo (✉) · P. Ferro · A. Tiziani
Department of Management and Engineering, University of Padova, Stradella San Nicola 3, 36100 Vicenza, Italy
e-mail: riccardo.cervo@unipd.it

F. Zucchi
Corrosion Study Centre A. Daccò, University of Ferrara,
Via G. Saragat, 4A, 44100 Ferrara, Italy

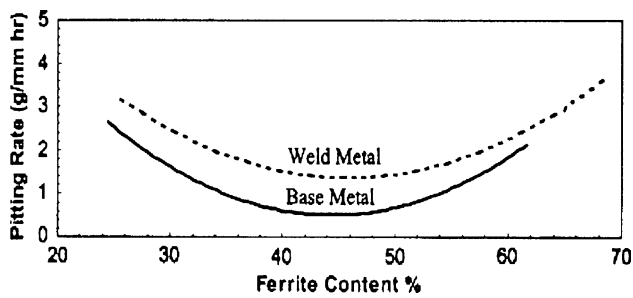


Fig. 1 Effect of ferrite content on pitting rate of SAF 2205 welded joint [16]

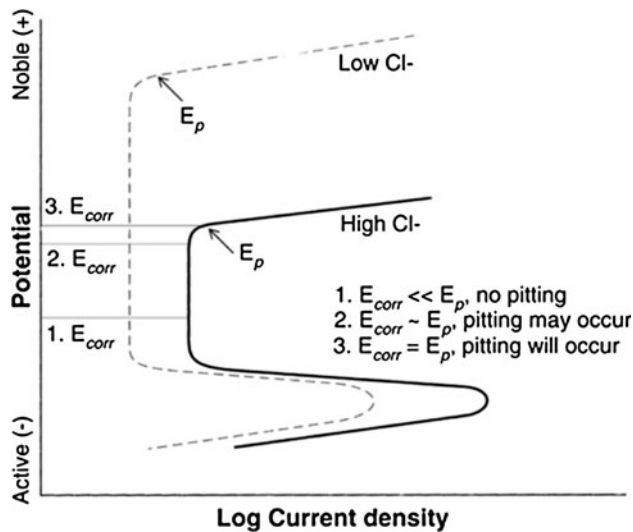


Fig. 2 Schematic representation of a polarization curve, determining the pitting corrosion risk [19]

Compared to the one-phase stainless steels, a complication arises when the pitting corrosion resistance of DSS and SDSS has to be evaluated because of the presence of two phases with different compositions and elemental partitioning.

The pitting resistance equivalent number ($PREN = \%Cr + 3.3\%Mo + (16 \div 30) \%N$) is the first parameter that can be considered when selecting the pitting corrosion resistance of austenitic/ferritic stainless steels. The literature offers a variety of standard formulas for PREN [1, 20–22], which are considered in detail in the experimental part of this study.

In the case of SDSS, since the corrosion resistance is controlled by the weaker phase, the PREN value of both the ferrite and austenite should be calculated [23, 24]. Moreover, the best corrosion resistance of the alloy is found when the two phases has the same PREN value. The partitioning behavior of chromium and molybdenum as well as the volume fraction of ferrite and austenite has a strong influence on the chemical composition of the two phases and then on each PREN value.

Since the ferrite volume fraction increases with increasing temperature, chromium and molybdenum become more diluted in this phase and thus the $PREN_{ferrite}$ decreases. On the other hand, a smaller austenite volume fraction leads to a higher concentration of nitrogen in γ phase, i.e., $PREN_{austenite}$ increases. To summarize, as the annealing temperature increases, PREN of austenite increases and PREN of ferrite decreases.

Consequently, Bernhardsson [25] and other authors such as Tuck et al. [26] and Tan et al. [27] suggested that the optimum annealing temperature can be reached when the two PREN-Temperature curves cross each other. In this condition the PREN reaches the maximum value for both the phases and the alloy reaches the best pitting corrosion resistance.

Because of the strict relationship between pitting corrosion behavior and the annealing temperature, the latter results to be a key parameter in order to determine the final corrosion properties of SDSS welded joints. Moreover, since the use of filler metal implies the presence of two different materials in terms of chemical composition (the base material [BM] and the fusion zone [FZ]), the welded joint is generally characterized by two different solubilization temperatures. Two annealing temperatures can be obtained and thus, when the optimum post-welding annealing temperature has to be chosen, a “trade-off” is required.

In the present part II, the pitting corrosion resistance of UNS S32750 welded joints (in the as-welded and annealed conditions) was experimentally evaluated by electrochemical measurements and ASTM G48 gravimetric tests. An effort has been made in order to correlate the main factors that affect pitting corrosion resistance of the SDSS welded joints (phase balance, intermetallic phases, partitioning of elements in ferrite and austenite, PREN), with the experimental data obtained from corrosion tests. Aim of this study is to determine the solution treatments conditions to obtain the best corrosion properties of the welded component. To author’s best knowledge, this topic, already treated in the literature [25] for the base material, is still lacking in the case of welded joints.

Experimental procedure

Materials and solubilization heat treatments

This study deals with UNS S32750 submerged-arc welded joints both in the as-welded and in the annealed conditions, as described in Part I.

To summarize, three post-weld solubilization treatment temperatures were considered: 1050 °C, 1100 °C, and 1150 °C. All the experimental results described in Part I

were used in this study, especially in terms of chemical composition obtained by optical spectrometer, microstructural features, and phase distribution obtained by metallographic analysis with a combination of Light Optical Microscope (LEICA), image analysis (by means of LEICA QWIN image analyzer), and environmental scanning electron microscope (FEI QUANTA 400) examinations; EDAX GENESIS energy dispersive spectroscopy (EDS) interfaced with ESEM was used to measure the content of substitutional alloying elements in austenite and ferrite (by using a 25 kV accelerating voltage).

PREN calculations

The pitting corrosion behavior was estimated on the basis of PREN calculations and microstructural analysis. A comparison with the experimental data obtained from corrosion tests was also carried out. The literature offers different formulas for PREN calculation [19, 20, 27]:

$$\text{PREN}_{16} = \%Cr + 3.3\%Mo + 16\%N \quad (1)$$

$$\text{PREN}_{20} = \%Cr + 3.3\%Mo + 20\%N \quad (2)$$

$$\text{PREN}_{30} = \%Cr + 3.3\%Mo + 30\%N \quad (3)$$

For stainless steels, the results included in references [26, 28–30] show that PREN_{16} gives a good correlation between corrosion resistance and chemical composition of DSS. Nevertheless, some authors [21, 27] suggest the use of the coefficient 20 or 30 for the nitrogen in order to emphasize the importance of this element in the behavior of the alloy, especially for SDSS.

Concerning this study, PREN was calculated, both for BM and FZ, by using Eqs. 2 and 3.

Pitting corrosion evaluation

The pitting corrosion resistance of the welded joints in the as-welded and in the annealed conditions was evaluated both by anodic polarization measurements and by gravimetric tests according to ASTM G48 standard method A [31]. Even if gravimetric tests provide general information about the pitting corrosion resistance of welded joints, they are unable to differentiate the different zones of the joint. Therefore, in order to study the corrosion performance of base and weld metal separately, anodic polarization measurements were also performed.

ASTM G48 gravimetric tests

Pitting corrosion resistance was also evaluated according to the Standard ASTM G48 method A, which is often applied in welding procedure qualifications. The specimens ($15 \times 15 \times 50$ mm), after being pickled for 5 min (10%

HF, 20% HNO_3 at 60 °C), were passivated in pure nitric acid for 15 min at room temperature. Finally, they were dipped for 24 h in ferric chloride reagent (100 g $\text{FeCl}_3 \cdot 6\text{H}_2\text{O}$ in 900 mL H_2O); exposure was performed at 50 ± 2 °C.

The corrosion rate was then calculated starting from the weight losses per unit of surface area according to the following equation:

$$\text{Corrosion rate} = \frac{Wt_i - Wt_f}{A} \quad (4)$$

where Wt_i and Wt_f are the weights of the sample measured before and after the test, respectively, and A is the exposed surface area. Weight losses were measured by means of a balance with a tolerance of 1 mg, and ultrasonic post-cleaning (5 min in acetone) was applied to the specimens.

Anodic polarization measurements

The anodic behavior of each specimen was analyzed. Since the HAZ was very narrow (about 100 μm), only the behaviors of BM and FZ (bottom pass) were differentiated.

Specimen preparation for the electrochemical tests was the same as described in the previous study (Part I) for the metallographic examinations. In particular, the final surface finishing was 6 μm . In order to prevent crevice corrosion the samples were passivated (15 min in pure nitric acid, room temperature) and a resin for edge retention was used.

The working electrode was built up using the samples embedded in epoxy resin, with a copper wire providing electrical contact.

The tests were carried out in a 3.5% NaCl open to air solution at 80 °C (which is approximately the critical pitting temperature of UNS S32750 [32]) by using a potentiostat–galvanostat (Princeton Applied Research Mod. 263A). The electrochemical cell was suspended in a water bath to control the solution temperature. An Ag/AgCl 3 M KCl electrode was used as the reference electrode, and the auxiliary electrode was a platinum sheet. The specimens were cleaned, degreased, and dried before starting the polarization tests. All data were recorded after an initial delay of 60 min for the specimen to stabilize at free corrosion potential; then the potential was increased from the free corrosion potential in the anodic direction at a scan rate of 1 mV/s until a current density of 1 mA/cm² was reached. The curves obtained are an average of three replicate tests of the same specimen. Finally, the corrosion behavior was evaluated by the absolute value of the pitting potential (E_p).

After polarization tests, each specimen was ultrasonic-cleaned with acetone, chemically etched with Beraha's etchant (80 mL H_2O , 30 ml HCl, 1 g $\text{K}_2\text{S}_2\text{O}_5$) and

examined at SEM to observe the pit morphology and the sites of pit nucleation, with a particular attention to the specific phase where the corrosion attack started.

Results and discussion

PREN analysis

It is known that the pitting resistance equivalent number could be used to quickly estimate the pitting corrosion resistance of superduplex stainless steels under sound plate or joint conditions (i.e.: absence of deleterious precipitates, secondary phases, etc.) [22, 24–30].

In this study, such index has been calculated for both the whole alloy and the single phases by using the data reported in the previous work (Part I). In particular, values for both BM and FZ were obtained and the results were summarized in Table 1.

It can be noted that in the as-welded conditions, very different values of $PREN_{austenite}$ and $PREN_{ferrite}$ were found in the FZ. On the other hand, the PREN values for the BM of the as-welded samples are similar to those of the annealed ones at a temperature of 1050 °C. This is in agreement with the fact that the BM in the as-received conditions was previously solubilized at 1070 °C.

Figure 3 shows the calculated values of $PREN_{30}$, both in BM and FZ, as a function of annealing temperature and phases.

Like expected, the solution-treated specimens show an increase in $PREN_{austenite}$ value with the increase of the annealing temperature; an inverse behavior was found for

$PREN_{ferrite}$. As described in the “Introduction,” the ferrite proportion increases with the annealing temperature so that its key elements such as chromium and molybdenum became more diluted. On the other hand, the decrease in austenite fraction results in a more concentrate content of nitrogen in it.

One can observe that the two $PREN_{30}$ curves, calculated in the FZ, cross each other at the annealing temperature of about 1125 °C. At this temperature the two phases reach the same $PREN_{30}$ value (42.5) so that it can be considered as the optimum value for the heat treatment of such a zone. This phenomenon is not capture for the BM if $PREN_{30}$ is used. However, by using the $PREN_{20}$ values, again the two curves cross each other (Fig. 4) and the same considerations made for the FZ can be transferred to the BM.

In this case, the optimum annealing temperature value was found to be 1070 °C ($PREN_{20} = 42$). It can be noted that for the BM UNS S32750 and by using the $PREN_{20}$ definition, Tan et al. [27] found a value of 1080 °C. When PREN is used as a criterion for estimating the pitting susceptibility of DSS and SDSS to pitting corrosion, it has to be remarked that one should consider the PREN of the weaker phase, which is generally different from the PREN calculated using the alloy composition (Table 1). The histograms of Fig. 5 collect the calculated $PREN_{20}$ and $PREN_{30}$ of the weaker phase for all the samples considered, referring to Table 1.

Figure 5 shows that a post-weld annealing treatment induces a remarkable increase of the minimum pitting resistance equivalent number in FZ (an increment of about 1.5 or 4.5 by using $PREN_{20}$ or $PREN_{30}$, respectively). Since the use of $PREN_{30}$ instead of $PREN_{20}$ gives more

Table 1 PREN values calculated for base and weld metal (S.T. solution treated)

Zone	Sample	Phase	$PREN_{20}$ (alloy) ^a	$PREN_{30}$ (alloy) ^a	$PREN_{20}$ (phase composition) ^b	$PREN_{30}$ (phase composition) ^b
FZ	As-welded	Ferrite	40.2	42.5	37.0	37.5
		Austenite			43.4	47.6
	S.T. 1050 °C	Ferrite	43.3	43.8		
		Austenite	38.6	41.9		
	S.T. 1100 °C	Ferrite	42.5	43.0		
		Austenite	38.7	42.2		
	S.T. 1150 °C	Ferrite	41.5	42.0		
		Austenite	38.9	42.7		
BM	As-welded	Ferrite	41.9	44.6	42.1	42.7
		Austenite			42.1	46.7
	S.T. 1050 °C	Ferrite	42.5	43.1		
		Austenite	41.6	46.1		
	S.T. 1100 °C	Ferrite	41.5	42.1		
		Austenite	42.6	47.3		
	S.T. 1150 °C	Ferrite	41.3	41.9		
		Austenite	43.0	47.9		

^a Calculated by using the chemical compositions obtained by optical spectrometer

^b Calculated by using compositions obtained by EDS analysis

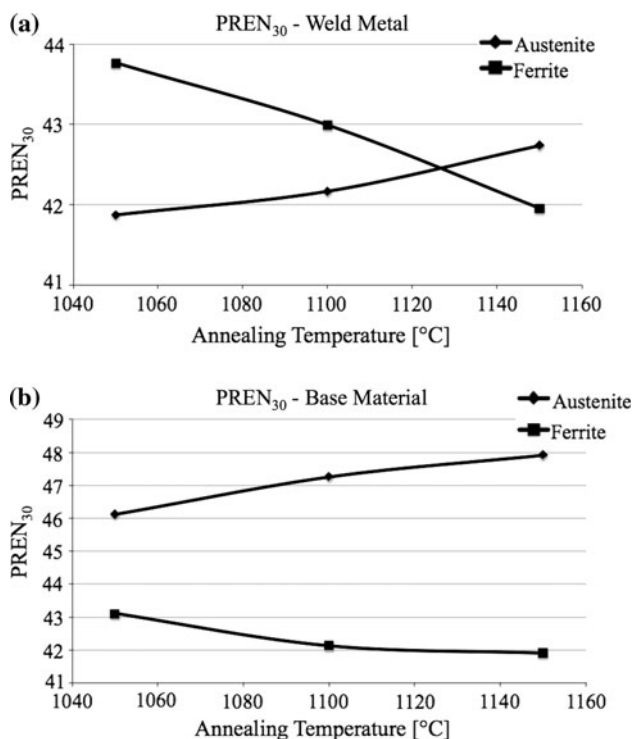


Fig. 3 Calculated values of $PREN_{30}$, both in FZ (a) and BM (b), as a function of annealing temperature and phases

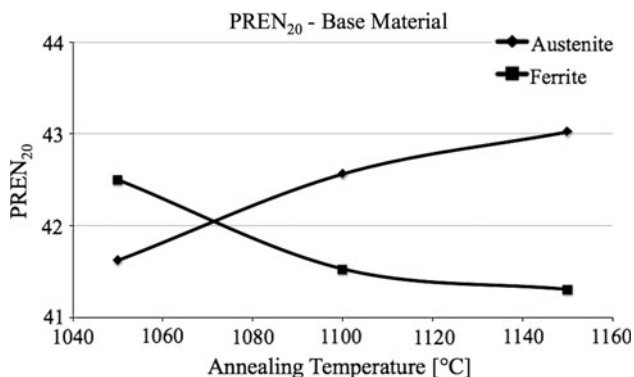


Fig. 4 Calculated $PREN_{20}$ for austenite and ferrite as function of annealing temperature—base material

importance to nitrogen (cf. Eqs. 2 and 3), which is mostly concentrated in austenite, the identification of weaker phase could change shifting from $PREN_{20}$ to $PREN_{30}$. For example, at an annealing temperature of 1050 °C, the weaker phase results to be austenite using $PREN_{20}$; nevertheless, considering $PREN_{30}$, the weaker phase becomes ferrite for the base material, because of the increased value of $PREN$ of austenite due to a higher weight attributed to nitrogen. Such observations are also applicable to the as-welded conditions and to the specimen annealed at 1150 °C: the shifting from austenite to ferrite as weaker phase is due to the increased importance of nitrogen moving from $PREN_{20}$ to $PREN_{30}$.

Finally, it can be observed that for the weld metal, the phases that result more susceptible to pitting corrosion (i.e., which have the lower $PREN_{30}$ value) are:

- *ferrite* in the as-welded conditions and in the specimen annealed at 1150 °C;
- *austenite* in the specimen annealed at 1050 °C and 1100 °C;

Concerning the BM, the weaker phase results to be *ferrite* in all the conditions.

Corrosion tests

ASTM G48 corrosion test results

The corrosion rates, measured according to the ASTM G48 corrosion test, are summarized in the histogram of Fig. 6, where the average value together with the standard deviation of three measurements are also reported.

Figure 7 shows the as-welded specimen after the ASTM G48 corrosion test; a deep corrosion attack can be seen in the welded zone.

The obtained experimental results confirmed the beneficial effect of a post-weld annealing treatment on the pitting corrosion resistance of UNS S32750 welded joints: a pronounced drop of the corrosion rates was found by comparing the as-welded specimen with the annealed ones. For the samples annealed at 1050 °C and 1100 °C the average corrosion rates are extremely low (lower than the acceptance threshold value of 4 g/m²); while, a slightly increase in the corrosion rate is observable in the sample annealed at 1150 °C, if compared with the previous ones.

Electrochemical measurements

The potentiodynamic anodic polarization technique was used to investigate the electrochemical behavior of the weld metal and base material separately. The average anodic polarization curves in 3.5% NaCl solution (open to air) at 80 °C are shown in Fig. 8.

The corrosion parameters, including free corrosion potentials (E_C) and pitting corrosion potentials (E_p) of all the specimens analyzed, are summarized in Table 2 (values are an average of at least three measurements).

All the specimens exhibited passivity in 3.5% NaCl at 80 °C. Concerning the as-welded specimens, it can be seen that the BM shows a higher pitting resistance than the FZ. However, after heat treatment, substantial changes in the average pitting potential of FZ have been detected. In particular, it was found that pitting potential value of the as-welded specimens (327 mV) is much lower than those of the annealed ones (947, 1045, 978 mV). Thus, a high

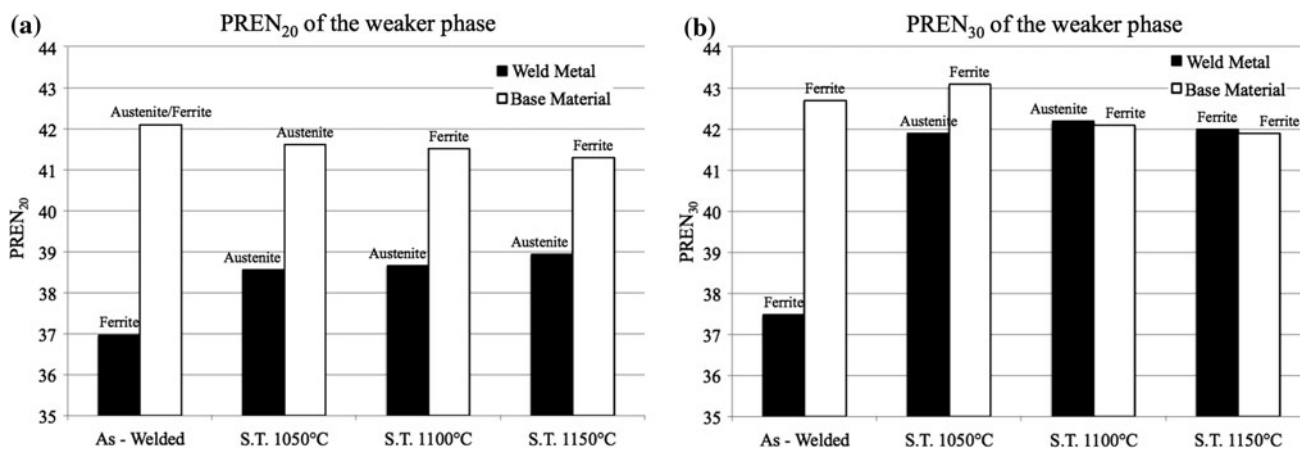


Fig. 5 Calculated values of PREN of the weaker phase as function of the specimen conditions (S.T. solution treated)

Fig. 6 Histogram showing the corrosion rates of the specimens after pitting corrosion test in 6 wt% FeCl solution, 24 h

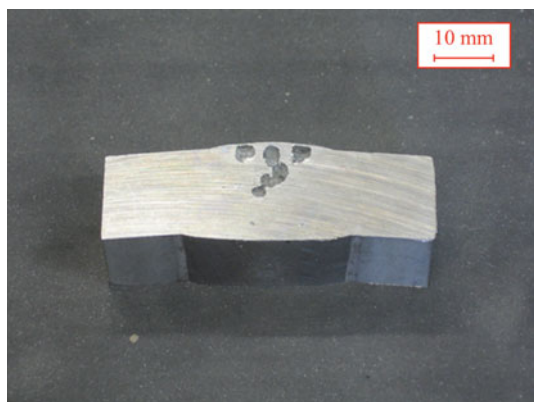
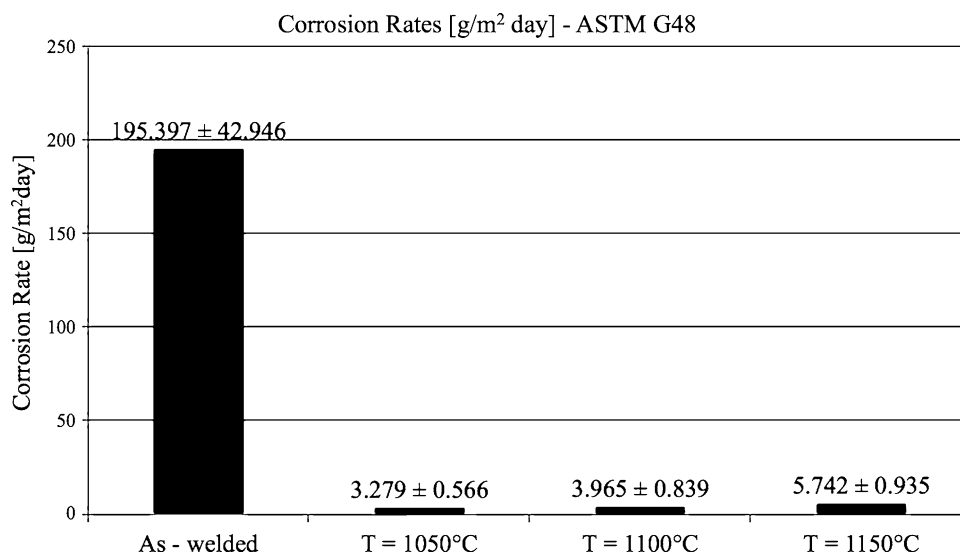


Fig. 7 As-welded specimen after the ASTM G48 test, 24 h

increase in the pitting potential can be easily noted in FZ after annealing treatment.

However, the data reported in Table 2 show that the average free corrosion potentials values of all the specimens

are not affected by significant changes (all the values lie in the range 160–280 mV versus Ag/AgCl).

The diagrams of Fig. 9 show all the pitting potentials data obtained by potentiodynamic tests as a function of specimen conditions, both for the base and the weld metal.

The data reported in Fig. 9a show that the as-welded specimen has the highest pitting potential. In fact, the base material in the as-welded conditions was previously solubilized at 1070 °C, which is the optimum annealing temperature as above defined (see Fig. 4). Concerning the annealing temperatures of 1050 °C and 1100 °C, the BM shows similar PREN₂₀ and E_p values. At the annealing temperature of 1150 °C, the E_p is affected by a slight decrease like the corresponding PREN₂₀ value (Fig. 4). If the FZ is considered (Fig. 7b), after solution treatment, the pitting potential increases for all the annealing temperatures; in particular the highest value is obtained at a temperature of 1100 °C. For annealing temperatures of 1050 °C and 1150 °C the pitting potential values show a

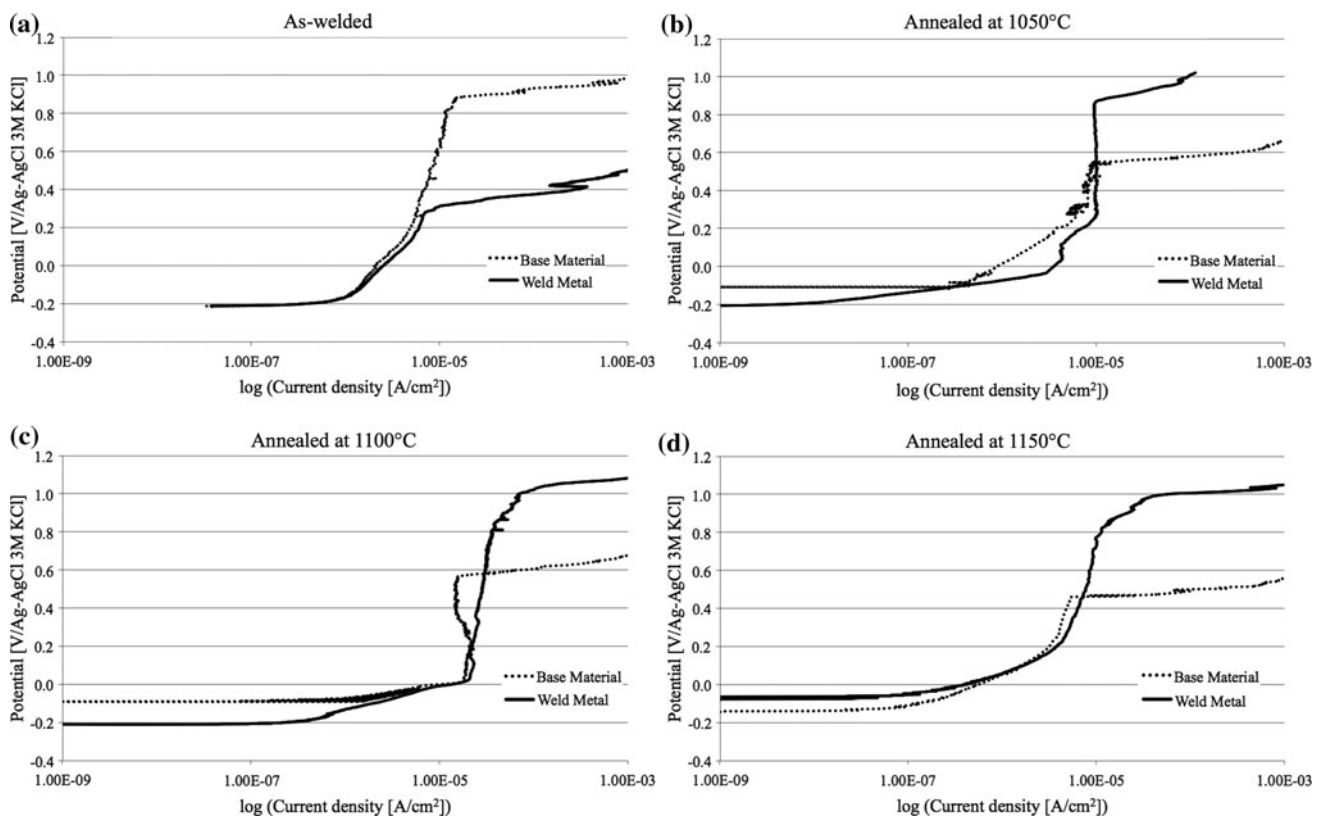


Fig. 8 Anodic polarization curves in 3.5% NaCl solution at 80 °C, open to air (a) as-welded specimen (b) annealed at 1050 °C (c) annealed at 1100 °C (d) annealed at 1150 °C

Table 2 Experimental values of pitting potential and free corrosion potential (vs Ag/AgCl 3 M KCl) of the specimens analyzed

Zone	Sample	E_C [mV versus Ag/AgCl 3 M KCl]		E_P [mV versus Ag/AgCl 3 M KCl]	
		Avg.	Std. Dev.	Avg.	Std. Dev.
FZ	As-welded	-228	25	327	20
	S.T. 1050 °C	-177	63	947	74
	S.T. 1100 °C	-249	39	1045	100
	S.T. 1150 °C	-160	36	978	55
BM	As-welded	-283	25	734	158
	S.T. 1050 °C	-157	12	521	71
	S.T. 1100 °C	-249	39	510	65
	S.T. 1150 °C	-201	64	413	83

slightly decrease compared to the previous one, like the calculated $PREN_{30}$ (Fig. 3).

To summarize, the ranking of the pitting corrosion resistance of the specimens analyzed is as follows:

weld metal : A.W. < S.T. 1050–1150 °C < S.T. 1100 °C

base material : S.T. 1150 °C < S.T. 1050–1100 °C < A.W. (S.T. 1070 °C)

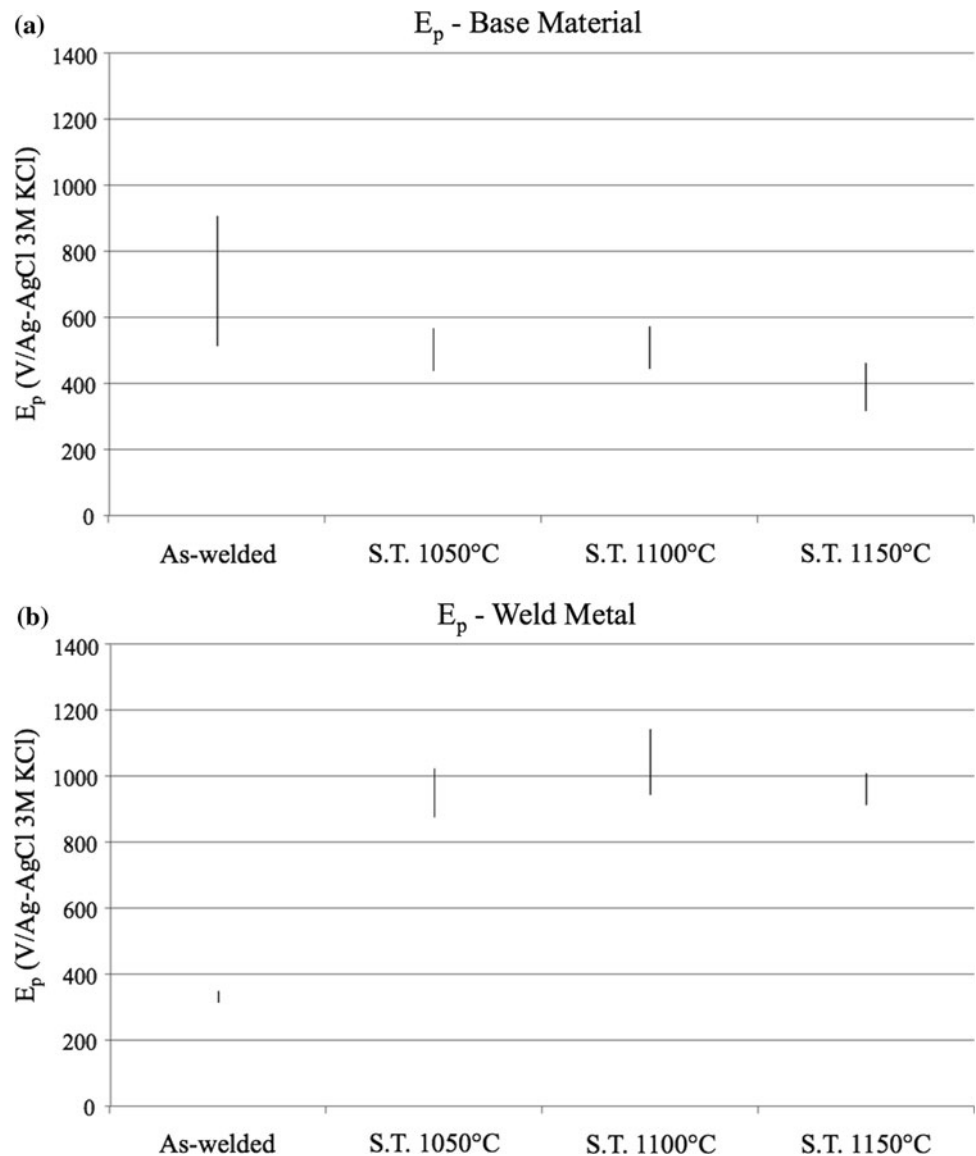
where A.W. is as welded, S.T. is solution treated.

Like reported in literature [33], the following exponential relationship between the calculated $PREN_{30}$ of weaker phase and experimental pitting potential was observed:

$$E_P = A \exp \cdot (B \cdot PREN_{30}) \quad (5)$$

where, for the welded metal, $A = 0.035$ (mV versus Ag/AgCl 3 M KCl) and $B = 0.243$. Figure 10 shows the data regarding the weld metal and the interpolation curve (Eq. 5).

Fig. 9 Pitting potential values obtained in 3.5% NaCl at 80 °C for base (a) and weld (b) metal (S.T. solution treated)



To summarize, Table 3 collects the main microstructural features that could affect pitting corrosion together with the measured pitting corrosion behavior of the welded joints analyzed in this study.

Pit morphology

Figure 11 shows the FZ SEM micrograph of the as-welded specimen after potentiodynamic tests.

Intensive selective pitting corrosion occurred in the ferrite phase of as-welded FZ. The corrosion process started at the ferrite/austenite grain boundaries or inside the ferrite grains. Pitting onset inside the ferrite grains could be attributed to the lower PREN₃₀ value of ferrite compared to that of austenite (37.5 against 47.6 of austenite). This is due to the low nitrogen content of the as-welded ferrite. It must be noted that the PREN₃₀ calculated by using the weld

metal composition (42.5) is quite higher than the correct PREN₃₀ value which corresponds to the one of the weaker phase (Table 1). The pitting onset at the ferrite/austenite grain boundaries (Fig. 11), may be due to the composition gradient inside the ferrite grains. In fact, during the solidification process, the δ -stabilizing elements concentrate more at the core than at the boundary of ferrite grains. As a consequence, the PREN values at the grain core are higher than those close to the grain boundaries. Thus, the grain boundary regions of the ferrite are more susceptible to localized pitting corrosion [34]. Moreover, the grain boundary is a transitional region characterized by a non-uniform and weaker passive film, which constitutes a preferential site for the pitting onset.

The BSE-SEM images collected in Fig. 12 show the pits detected in the welded metal of the annealed specimens after potentiodynamic tests.

Fig. 10 Pitting potential versus $PREN_{30}$ of the weaker phase (weld metal)

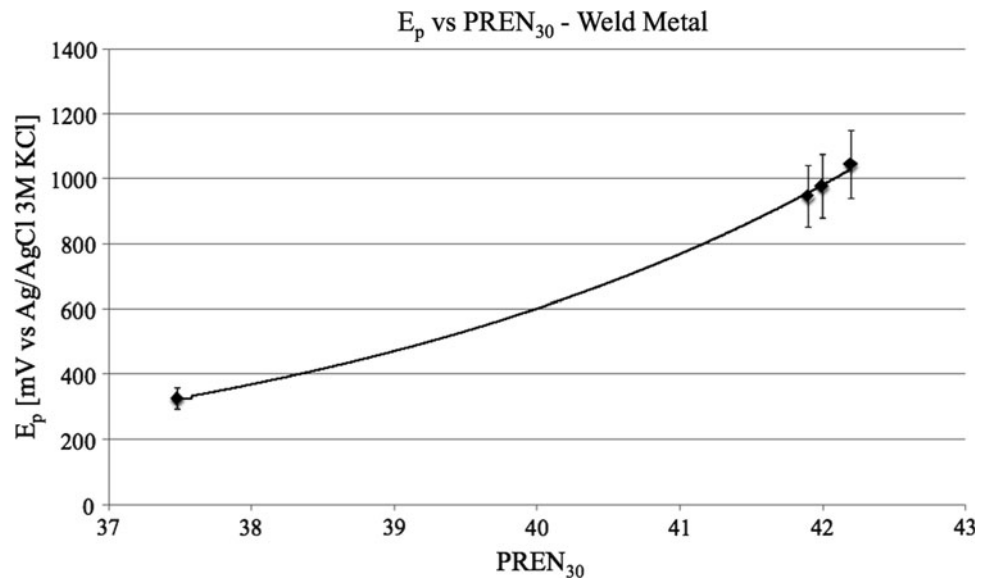


Table 3 Summary of the main microstructural features and experimental pitting corrosion behavior of the welded joints analyzed in this study

Sample	Zone	Microstructure			Experimental pitting corrosion behavior	
		δ/γ ratio	Precipitates detected (zone)	Calculated $PREN_{30}$ (weaker phase)	Average E_p (mV vs Ag/AgCl 3 M KCl)	Average corrosion rate (g/m^2 day)
As-welded	FZ	1.07	–	37.5 (ferrite)	327	195.397
	BM	0.89	Cr ₂ N (HAZ)	42.7 (ferrite)	734	
S.T. 1050 °C	FZ	0.53	–	41.9 (austenite)	947	3.279
	BM	0.80	–	43.1 (ferrite)	521	
S.T. 1100 °C	FZ	0.65	–	42.2 (austenite)	1045	3.965
	BM	1.03	–	42.1 (ferrite)	510	
S.T. 1150 °C	FZ	0.99	–	42.0 (ferrite)	978	5.742
	BM	1.09	–	41.9 (ferrite)	413	

FZ fusion zone, BM base material

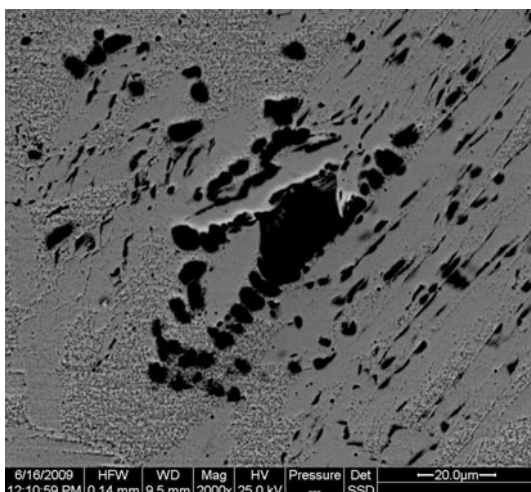


Fig. 11 Aspect of the pitting attack revealed in the welded zone of the as-welded specimen after potentiodynamic test in 3.5% NaCl at 80 °C ($\times 2,000$)

It must be first noted that in the annealed specimens the pitting attack is less intense than in the as-welded sample. Second, by analyzing the images in Fig. 12, the phase affected by the pitting attack results to be:

- austenite in the sample annealed at 1050 °C (Fig. 12a) (austenite has a lower calculated $PREN_{30}$ value than ferrite (41.9 against 43.8));
- mainly austenite but also ferrite in the sample annealed at 1100 °C (Fig. 12b) (in fact the calculated $PREN_{30}$ value for both phases are slightly similar (42.2 and 43.0 for austenite and ferrite, respectively));
- both austenite and ferrite in the sample annealed at 1150 °C (Fig. 12c); (the calculated $PREN_{30}$ values in this case are 42.0 and 42.7 for ferrite and austenite, respectively).

The SEM micrographs collected in Fig. 13 show the aspect of the etched surface of BM after potentiodynamic test and at different magnifications.

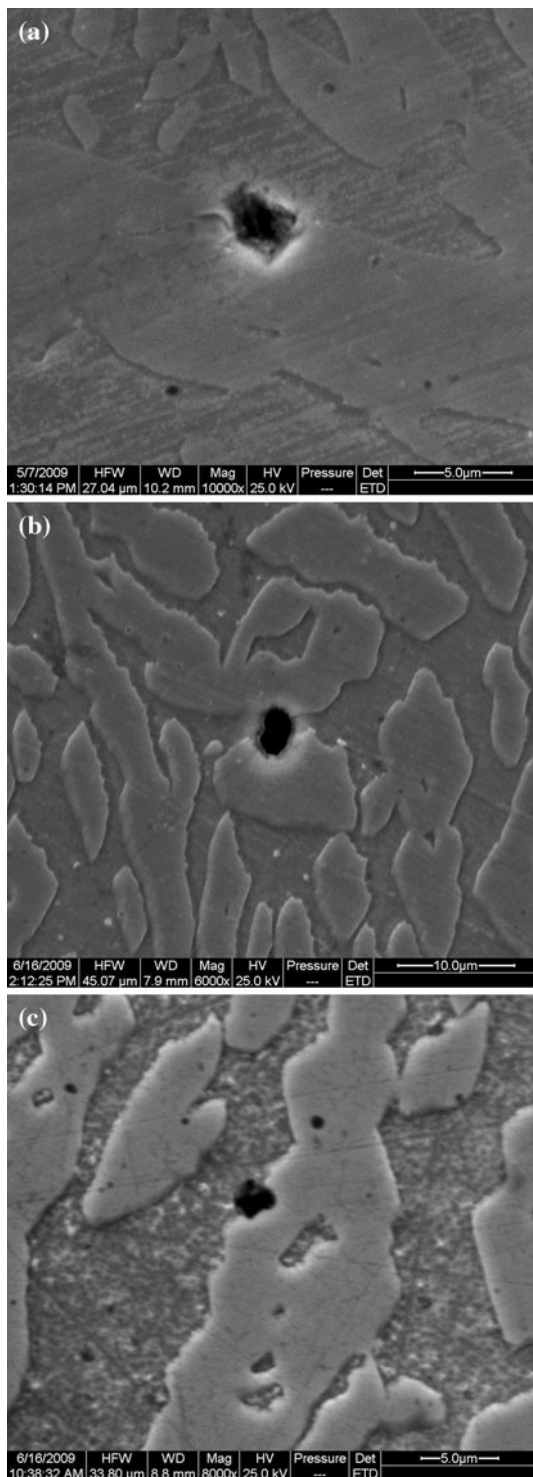


Fig. 12 BSE-SEM images of the pits revealed in the welded zone of the annealed specimens after potentiodynamic tests in 3.5% NaCl at 80 °C (**a** $\times 10,000$, **b** $\times 6,000$, **c** $\times 8,000$)

Pits were observed preferentially in the ferrite phase of the base material for all the samples conditions. As a matter of fact, the $PREN_{30}$ of ferrite is always lower than that of austenite. The pitting attack starts both on the ferrite/

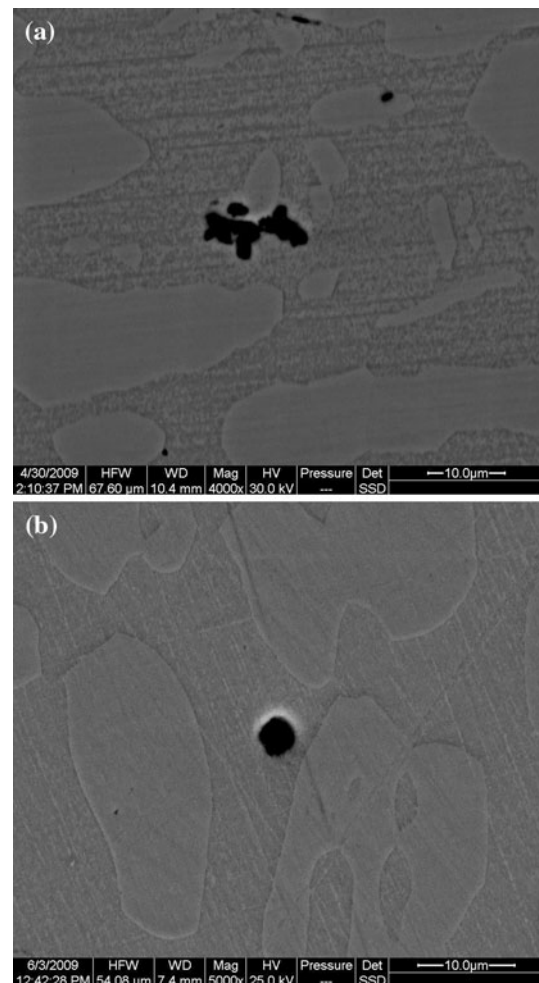


Fig. 13 Pit morphologies found after potentiodynamic test in 3.5% NaCl at 80 °C in the base material (**a** specimen annealed at 1050 °C, $\times 4,000$; **b** specimen annealed at 1150 °C, $\times 5,000$)

austenite grain boundaries (Fig. 13a) and inside the ferrite grains (Fig. 13b). However, it has to be noted that in the as-welded and in the solution treated at 1050 °C specimens, sometimes pits were observed also in the austenite phase (Fig. 13a) this phenomenon can be captured only if $PREN_{20}$ is taken into account. In fact its value is lower (or equal, in the case of the as-welded specimen) in austenite phase than in ferrite.

Overall discussion on pitting corrosion behavior

As-welded specimen shows the maximum corrosion rate in terms of weight losses per day after ASTM G48 test; the pitting attack is heavily concentrated in the welded zone, which has a lower pitting potential and $PREN_{30}$ compared to the base material. The ferrite and austenite phase of the welded zone have approximately the same chromium and molybdenum content, but austenite is enriched in nitrogen, which raises significantly its $PREN$. Due to the very low

PREN value of ferrite, intense pitting attack takes place in this phase pertaining to the as-welded FZ.

After post-welding solution annealing, a high decrease of the corrosion rates occurred. This phenomenon is mainly due to the concurrent increase of both the pitting potential (from 327 mV to values greater than 950 mV versus Ag/AgCl 3 M KCl) and the calculated $PREN_{30}$ of the FZ (from a value of 37.5 to values up to 42). The ferrite phase in FZ, by enriching in chromium and molybdenum, increases its PREN value, whereas the content of these elements in austenite decreases. Moreover, the precipitates detected in the heat-affected zone of the as-welded specimen (described in the previous work and which could be deleterious for pitting corrosion resistance of the joint) tend to dissolve after all the annealing treatment.

Concerning the annealed samples, the best pitting corrosion resistance, in terms of weight losses per day, was reached at annealing temperatures of 1050 °C and 1100 °C. This can be justified by combining the results obtained from potentiodynamic tests. The highest pitting potential in the weld metal was obtained with the specimen treated at 1100 °C, while, regarding the base material, the most favorable pitting behavior was found with the specimens in the as-welded conditions (i.e.: previously solubilized at 1070 °C).

However, among the annealed samples, the corrosion rate of the specimen heat-treated at 1150 °C shows a slightly decrease; as a matter of fact, the E_p and PREN decrease both in the base material and in the FZ. In addition, concerning the weld metal, an exponential relationship between the calculated values of $PREN_{30}$ and experimental values of E_p was found.

A good agreement between the predicted weaker phase (by using PREN values) and experimental observations was found in all the analyzed specimens.

In this study, the calculated optimum annealing temperatures corresponds to 1070 °C and 1125 °C for BM and FZ, respectively. As a consequence, an intermediate annealing temperature of 1100 °C results to be optimal for the annealing heat treatment of UNS S32750 welded joints.

Conclusions

In this study, the pitting corrosion behavior of UNS S32750 submerged-arc welded joints was analyzed. The obtained results are strictly correlated to the microstructure and partitioning of elements treated in the previous work (Part I) for the same samples.

Since in the FZ of as-welded specimens, substitutional elements (such as chromium, molybdenum, and nickel) are homogeneously distributed in both phases, while nitrogen

is supposed (according to results found in the literature) to be heavily concentrated in austenite, $PREN_{30}$ of ferrite results lower (37.5) if compared with that of austenite (47.6).

During the heat treatment the PREN value of the two phases follows the trend found by Bernhardsson [25]. In particular, the FZ $PREN_{30}$ reaches the maximum value around 1125 °C, while the BM $PREN_{20}$ reaches the maximum value at a temperature of 1070 °C (as-received conditions).

Finally, the following conclusions about the pitting corrosion resistance of the analyzed welded joints can be collected:

1. In the as-welded conditions, the PREN of the welded zone is lower than the PREN of the base material, because of the low chromium, molybdenum and nitrogen content of ferrite pertaining to the fusion zone, which is characterized by a deep pitting corrosion attack after experimental corrosion tests.
2. After post-welding heat treatment the pitting corrosion resistance of the FZ increases because of the different elemental distribution between the two phases.
3. The experimental corrosion behavior of examined samples shows that PREN calculated from bulk composition is unlikely to be a good guide to assess pitting resistance of superduplex stainless steels; nevertheless, a better understanding can be achieved through calculating PREN values for the two phases. In fact, like reported in the literature [33], an exponential relationship between experimental pitting potential (in 3.5% NaCl solution at 80 °C) and calculated $PREN_{30}$ of weaker phase has been found in this study; in particular, this relation has been extended to the case of weld metal.
4. The best pitting resistance was found experimentally in samples treated at 1100 °C for the FZ and at 1070 °C for the BM (as-received conditions) which are temperature values very close to those theoretically calculated by PREN analysis. Therefore, in order to obtain the best pitting resistance of the whole joint, an intermediate annealing temperature of 1100 °C is proposed for post-weld treatment.
5. Additional microstructural factors, first the presence of precipitates, may need to be considered to fully understand the relative pitting resistances of UNS S32750 welded joints.

Acknowledgements The authors gratefully acknowledge the experimental support provided by Mr. Giacomo Mazzacavallo, Dr. Enrico Della Rovere, and Dr. Vincenzo Grassi. Special thanks are also due to Rivit S.p.A. (Caltrano, VI—Italy) for the materials supply and welding.

References

1. Nilsson JO (1992) *Mater Sci Technol* 8:685
2. Atamert S, King JE (1991) *Acta Metall Mater* 39(3):273
3. Bonollo F, Tiziani A, Ferro P (2009) *Advances in duplex stainless steels*, chap 4. ISTE LTD, London
4. Tavares SSM, Pardal JM, Lima LD, Bastos IN, Nascimento AM, de Souza JA (2007) *Mater Charact* 58:610
5. Taban E (2008) *J Mater Sci* 43:4309. doi:[10.1007/s10853-008-2632-z](https://doi.org/10.1007/s10853-008-2632-z)
6. Sathiya P, Aravindan S, Soundararajan R, Noorul Haq A (2009) *J Mater Sci* 44:114. doi:[10.1007/s10853-008-3098-8](https://doi.org/10.1007/s10853-008-3098-8)
7. Migiakis K, Papadimitriou GD (2009) *J Mater Sci* 44:6372. doi:[10.1007/s10853-009-3878-9](https://doi.org/10.1007/s10853-009-3878-9)
8. Ogawa T, Koseki T (1989) *Weld J* 68:181
9. Liao J (2001) *ISIJ Int* 41(5):460
10. Liou H-Y, Hsieh R-I, Tsai W-T (2002) *Mater Chem Phys* 74:33
11. Nilsson JO, Karlsson L, Anderson JO (1995) *Mater Sci Technol* 11:276
12. Kwok CT, Fong SL, Cheng FT, Man HC (2006) *J Mater Process Technol* 176:168
13. Kordatos JD, Fourlaris G, Papadimitriou G (2001) *Scripta Mater* 44:401
14. Bautista A, Blanco G, Velasco F, Martinez MA (2007) *Constr Build Mater* 21:1267
15. Garzon CM, Serna CA, Brandi SD, Ramirez AJ (2007) *J Mater Sci* 42:9021. doi:[10.1007/s10853-007-1881-6](https://doi.org/10.1007/s10853-007-1881-6)
16. Sun Z, Kuo M, Annergren I, Pan D (2003) *Mater Sci Eng A* 356:274
17. Muthupandi V, Bala Srinivasan P, Seshadri SK, Sundaresan S (2003) *Mater Sci Eng A* 358:9
18. Ferro P, Tiziani A, Bonollo F (2008) *Weld J* 87:298
19. Pohjanne P, Carpén L, Hakkarainen T, Kinnunen P (2008) *J Constr Steel Res* 64:1325
20. Herbsleb G (1982) *Werkst Korros* 33:334
21. Lorenz K, Medawar G (1969) *Thyssen Forschung* 1:97
22. Dölling R, Neubert V, Knoll P (1991) In: *Proceedings of the duplex stainless steels conference*, vol 91. Beaune, France, pp 1341–1351
23. Vannevik H, Nilsson JO, Frodigh J, Kangas P (1996) *ISIJ Int* 36(7):807
24. Weber L, Uggowitzer PJ (1998) *Mater Sci Eng A* 242:222
25. Bernhardsson S (1991) In: *Proceedings of the duplex stainless steels conference*, vol 185. Beaune, France
26. Tuck CDS, Sykes JM, Garfias-Mesias LF (1994) In: *4th International conference of duplex stainless steels*, Glasgow, paper 15
27. Tan H, Jiang Y, Deng B, Sun T, Xu J-L, Li J (2009) *Mater Charact*. doi:[10.1016/j.matchar.2009.04.009](https://doi.org/10.1016/j.matchar.2009.04.009)
28. Van Bennekom A (1998) *Steel World* 54
29. Garfias-Mesias LF, Sykes JM, Tuck CDS (1996) *Corros Sci* 38:1319
30. Vannevik H, Nilsson JO, Frodigh J, Kangas P (1996) *ISIJ Int* 36:807
31. *Annual book of ASTM standards*, ASTM G48-03, 2003, ASTM
32. Deng B, Jiang Y, Gong J, Zhong C, Gao J, Li J (2008) *Electrochim Acta* 53:5220
33. Merello R, Botana FJ, Botella J, Matres MV, Marcos M (2003) *Corros Sci* 45:909
34. Batista SRF, Kuri SE (2004) *Methods Mater* 51(3):205